Supplementary Information:

An Lsr2-like xenogeneic silencer confers immunity against AT-rich bacteriophage infection

Biel Badia Roigé[a,b], Nadiia Pozhydaieva[c,d], Ombeline Rossier[e], Konstantinos Kalogeropoulos[c,d,f,g], Christophe Regeard[e], Karen L. Maxwell[h], Stan J. J. Brouns[c,d], Eugen Pfeifer[i,j], Julia Frunzke[a,b*]

[a]Institute of Bio- und Geosciences, IBG-1: Biotechnology, Forschungszentrum Jülich, Jülich, Germany

[b]HHU Düsseldorf, Faculty of Mathematics and Natural Sciences Institute of Microbial Interactions, Heinrich-Heine-University Düsseldorf, Düsseldorf, Germany

[c]Department of Bionanoscience, Delft University of Technology, The Netherlands

[d]Kavli Institute of Nanoscience, 2629 HZ Delft, The Netherlands

[e]Université Paris-Saclay, CEA, CNRS, Institute for Integrative Biology of the Cell (I2BC), 91198, Gif-sur-Yvette, France

[f]Department of Biotechnology and Biomedicine, Technical University of Denmark, Denmark

[g]Center for Translational Protein Design, Technical University of Denmark, Søltofts Plads, DK-2800, Kongens Lyngby, Denmark

[h]Department of Biochemistry, University of Toronto, Toronto, Ontario, Canada

[i]Université Paris-Saclay, INRAE, AgroParisTech, MICALIS, 78350 Jouy-en-Josas, France

[j]Université Paris-Saclay, INRAE, MetaGenoPolis, 78350 Jouy-en-Josas, France

*Corresponding author: Julia Frunzke (j.frunzke@fz-juelich.de)

Overview:

Supplementary Fig. 1 | CgpS is required within the AT-rich CGP3 context for defense against JeanGrey.

Supplementary Fig. 2 | Low-abundance JeanGrey proteins approach the detection limit.

Supplementary Fig. 3 | Validation of additional target regions, further replicates of main targets, and technical limitations of ChAP-seq under infection conditions.

Supplementary Fig. 4 | Time-resolved fluorescence microscopy of CgpS–Venus during JeanGrey infection.

Supplementary Fig. 5 | Global transcriptional changes during JeanGrey infection.

Supplementary Fig. 6 | *C. glutamicum*–encoded Lsr2 forms a distinct clade separate from *Mycobacterium*- and phage-encoded homologs.

Supplementary Table 1 | Strains used and generated in this study.

Supplementary Table 2 | Plasmids used and generated in this study.

Supplementary Table 3 | Genome annotation of bacteriophage JeanGrey.

Supplementary Table 4 | Oligonucleotides used in this study for cloning, sequencing, (RT)-qPCR, and EMSA studies.

Supplementary Table 5 | Raw values and differential protein abundance during phage infection in-CGP3 (a, c) and +CGP3 (b, d) cells.

Supplementary Table 6 | Overview of EMSA analysis of phage DNA regions tested with increasing CgpS concentrations.

Supplementary Table 7 | RNA-seq analysis across all targets and time points.

Supplementary Table 8 | Genome sequences encoding Lsr2 homologues included in phylogenetic analysis.

Supplementary Table 9 | Annotation of genomic regions encoding Lsr2 homologues.

Supplementary Video 1 | Time-lapse imaging of-CGP3 infection with JeanGrey.

Supplementary Video 2 | Time-lapse imaging of +CGP3 infection with JeanGrey.

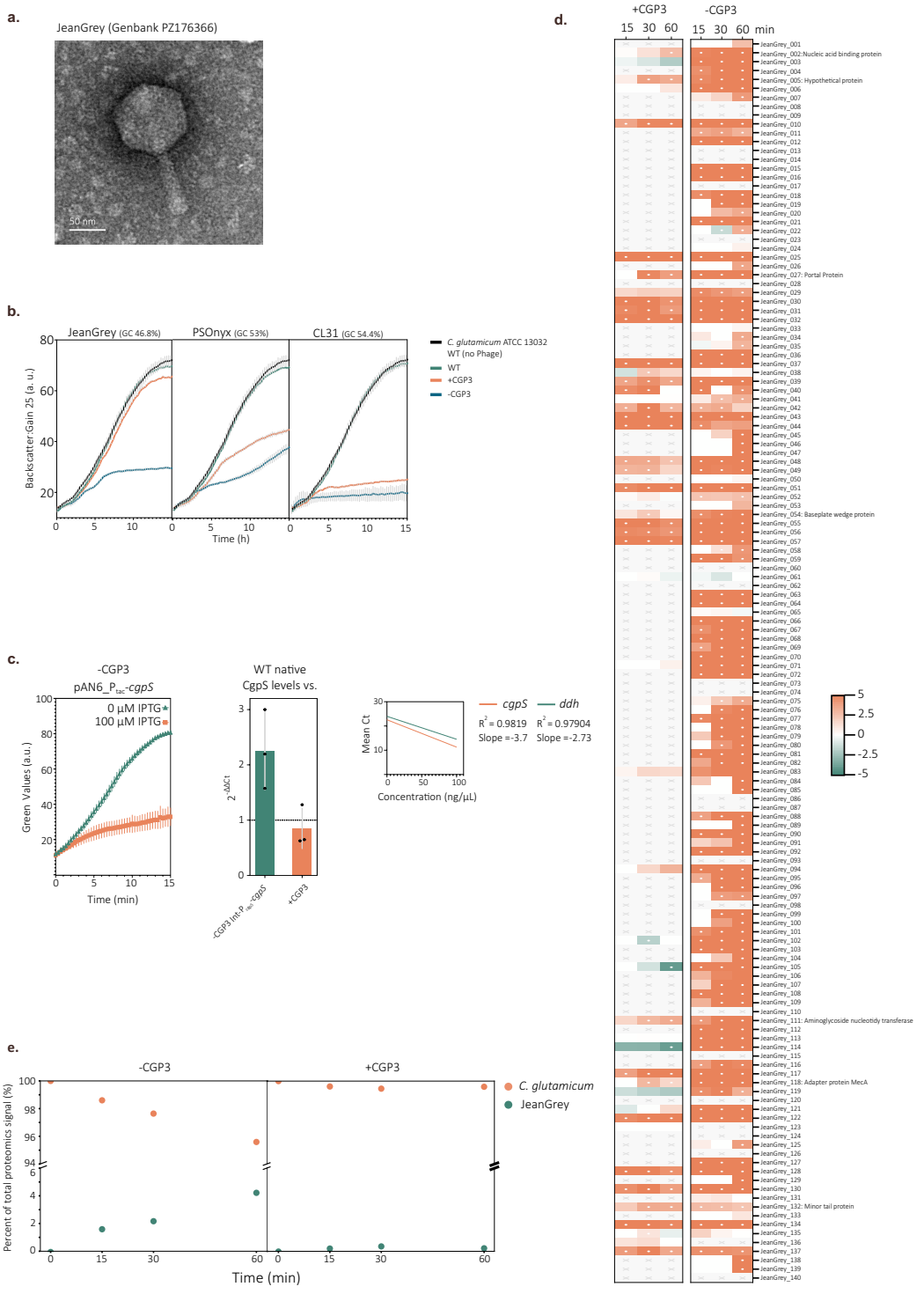

Supplementary Fig. 1 | CgpS is required to defend against infection of the AT-rich phage JeanGrey. (a) Transmission electron micrographs of the newly isolated phage JeanGrey. Scale bar, 50nm. (b) Phage infection assays using JeanGrey, PSOnyx, and CL31 on *C. glutamicum* strains carrying different CGP3 backgrounds: CGP3 lacking the RM system (+CGP3; orange), wild type containing the complete CGP3 region (WT; green, infected; black, non-infected), and a complete CGP3 deletion (-CGP3; blue). Growth over the first 15h is shown (n=3 biological replicates). Error bars in grey represent SD. (c) Left, overexpression of *cgpS* in the-CGP3 background results in severe growth defects. Right, chromosomal reintegration of *cgpS* in the-CGP3 background shows reduced expression levels due to autoregulation. Error bars represent SD. Bars indicate mean values. (n=3 biological replicates ; n=2 technical replicates). (d) Time-resolved phage proteome analysis over 60min in +CGP3 (left) and-CGP3 (right) backgrounds. Proteins showing statistically significant changes in +CGP3 are indicated by gene name and annotated function (n=3 biological replicates). Dots within the samples indicate statistically significant differences ($P < 0.05$), determined using a two-tailed Student's t-test. (e) Relative contribution of detected proteins expressed as percentage of total signal intensity. Orange dots represent host-encoded proteins, and green dots represent phage-encoded proteins. The combined signal of both groups equals 100% in each sample (0, 15, 30, and 60 min).

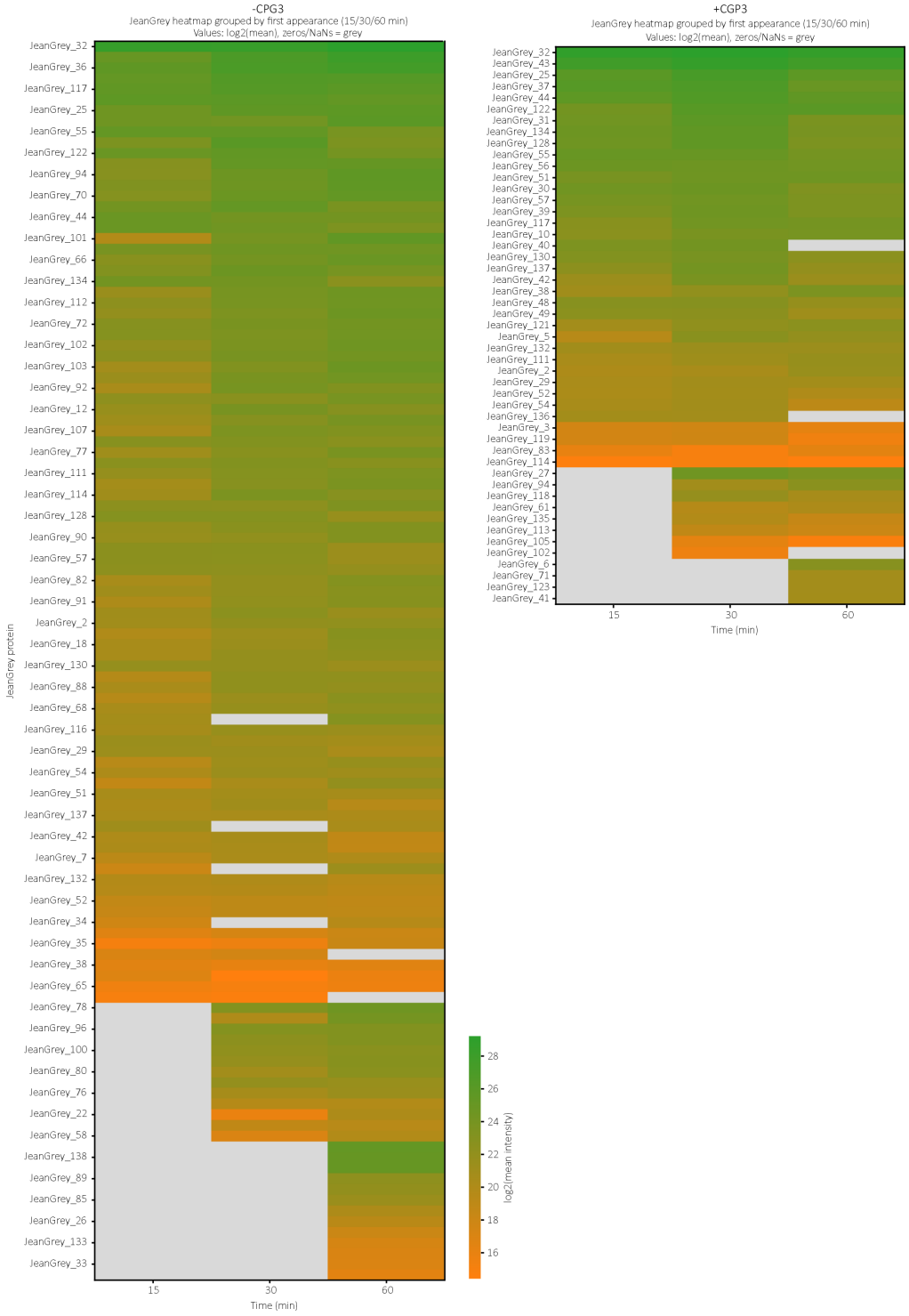

Supplementary Fig. 2 | Low-abundance JeanGrey proteins approach the detection limit. Log_2 mean protein intensities at 15, 30, and 60 min post infection (n=3 biological replicates). Left,-CGP3 background; right, +CGP3 background. Calculation of log_2 fold changes at very low protein abundances resulted in apparent negative values for several phage proteins (JeanGrey_105, JeanGrey_110, JeanGrey_114 and JeanGrey_119) in +CGP3. Examination of the corresponding mean log_2 intensities showed that these signals were close to the detection limit, consistent with minimal phage protein production rather than true downregulation.

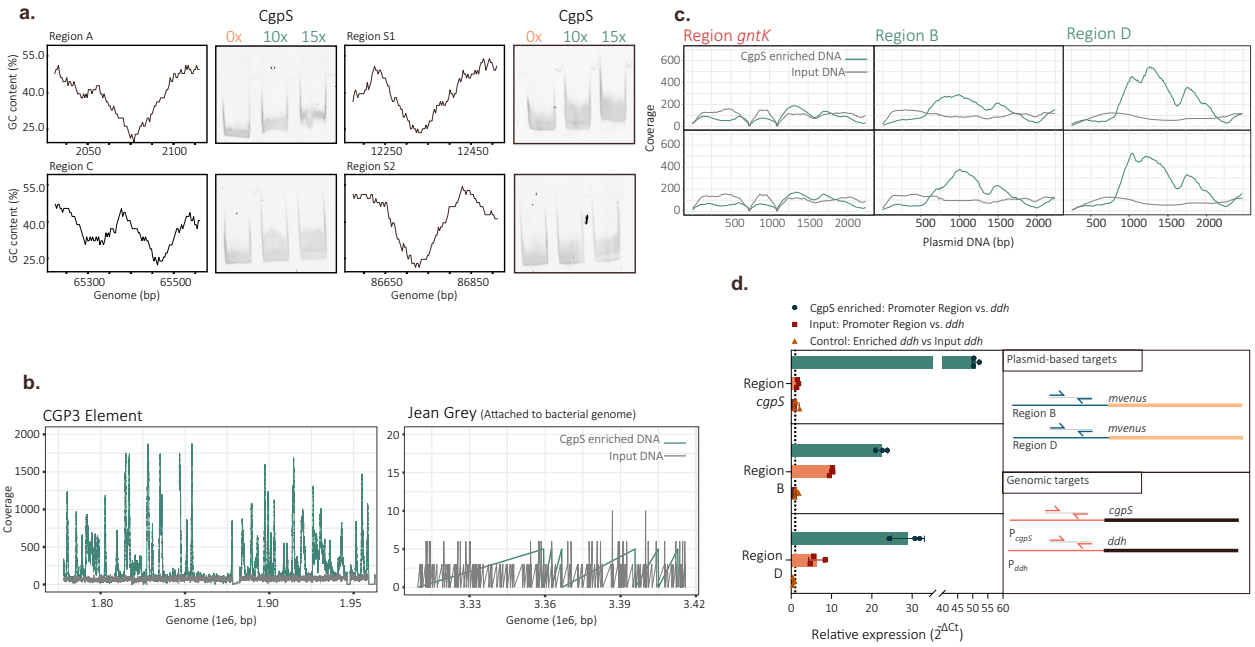

Supplementary Fig. 3 | Validation of additional target regions, further replicates of main targets, and technical limitations of ChAP-seq under infection conditions. (a) Additional JeanGrey regions (regions A and C, left; regions S1 and S2, right) analyzed by EMSA to validate CgpS binding in vitro. Fragment GC content and mobility shifts at increasing CgpS concentrations (0×, 10× and 15× molar excess) are shown. (b) ChAP-seq under infection conditions yields non-informative enrichment profiles for phage DNA. Left, CgpS binding peaks across the CGP3 region. Right, sequencing reads predominantly mapping to phage DNA. Input samples are shown in grey and enriched samples in green. (c) Two independent biological replicates of plasmid-based ChAP-seq for regions *gntK*, as well as phage regions B and D. (d) qPCR validation of ChAP-seq enrichment of B and D regions. Left, comparison of enriched samples to the respective region of interest normalized to *ddh* (green circles); comparison of plasmid-based targets relative to genomic targets (orange squares); and comparison of *ddh* levels between CgpS enriched and input samples (brown triangles). Bars indicate mean values. Error bars represent SD. Right, schematic representation of the analyzed regions.

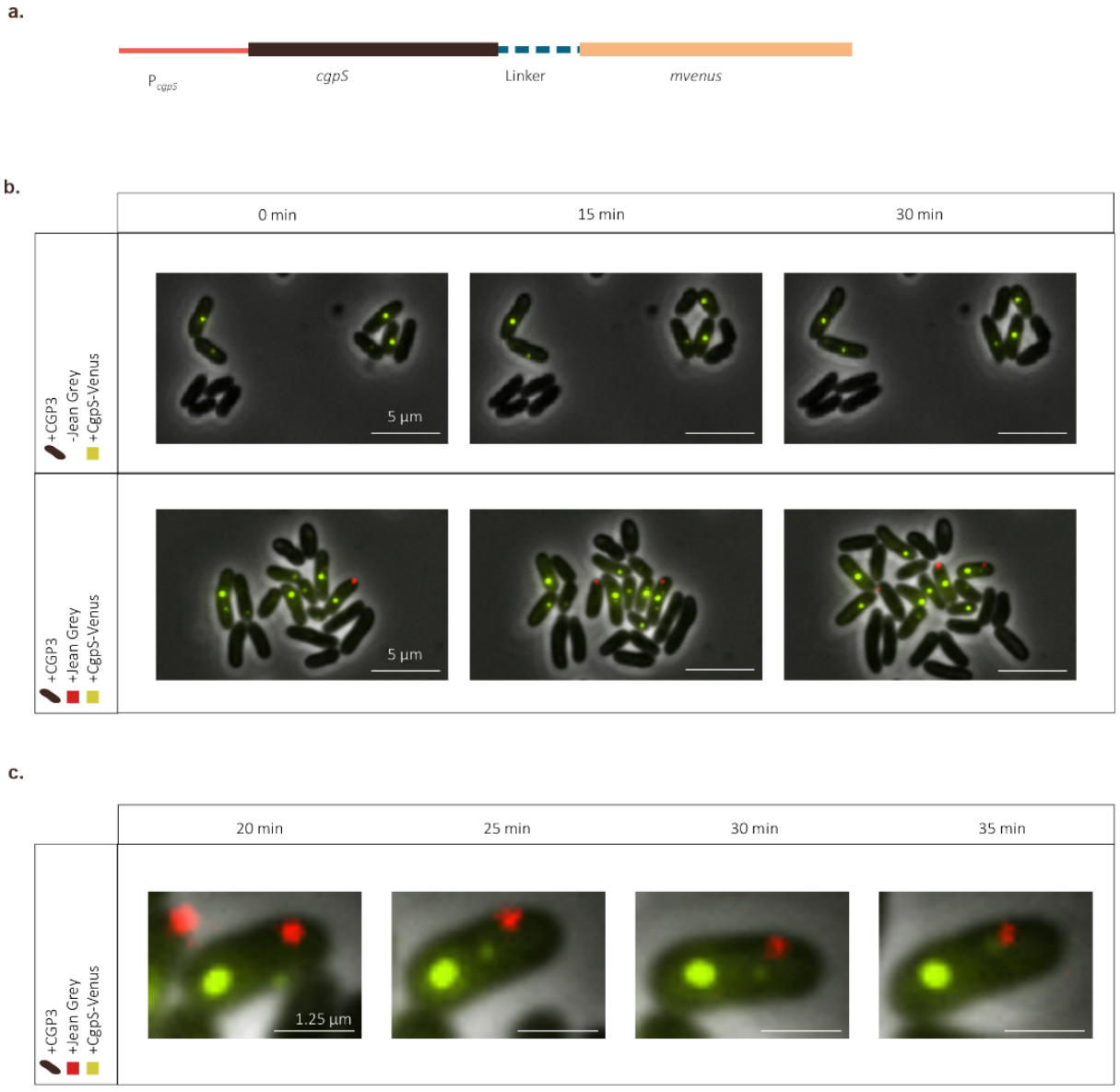

Supplementary Fig. 4 | Time-resolved fluorescence microscopy of CgpS–Venus during JeanGrey infection. Cells were visualized in a microfluidic chamber and exposed to short pulses of JeanGrey phage (10^7 PFU ml^{-1}) diluted in LB. (a) Schematic of the fusion construct. (b) Fluorescence microscopy images at 0, 15, and 30 min in the absence (top) and presence (bottom) of JeanGrey. CgpS–Venus is shown in yellow. Phage particles are visualized by Alexa Fluor–based capsid staining (red). Scale bar, 5 µm. (c) Higher-magnification time series (20–35 min) showing an attached phage particle (red) and re-localization of CgpS–Venus (yellow punctum) towards the zones of phage DNA injection. Scale bar, 1.25 µm.

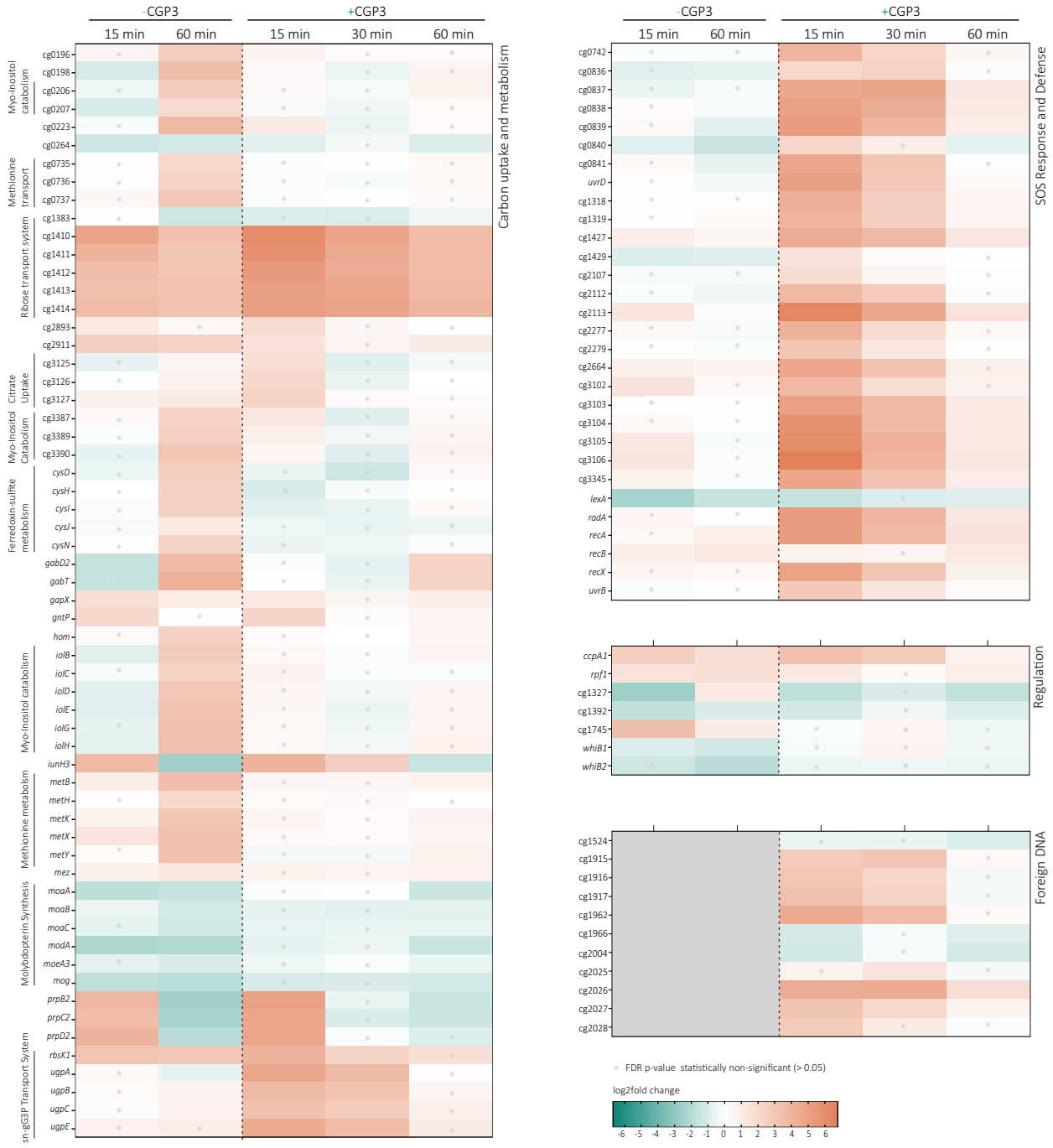

Supplementary Fig. 5 | Global transcriptional changes during JeanGrey infection. Transcriptome profiling of infected versus uninfected cells in +CGP3 and -CGP3 backgrounds at 15, 30, and 60 min, post infection. Differential expression is shown as $\log_2$ fold change. Genes are grouped into four functional categories: carbon uptake and metabolism (left), and SOS/defense response, regulatory functions, and foreign DNA expression (right). Previously characterized metabolic genetic clusters are indicated on the left side of each panel with its functions. Grey stars denote genes that did not reach statistical significance at the respective time point (false discovery rate (FDR) > 0.05) and were excluded from downstream analysis. All other displayed genes meet the significance threshold (FDR < 0.05). FDR-adjusted P values were calculated in CLC Genomics Workbench using empirical analysis of differential gene expression. Data are derived from n = 2 biological replicates.

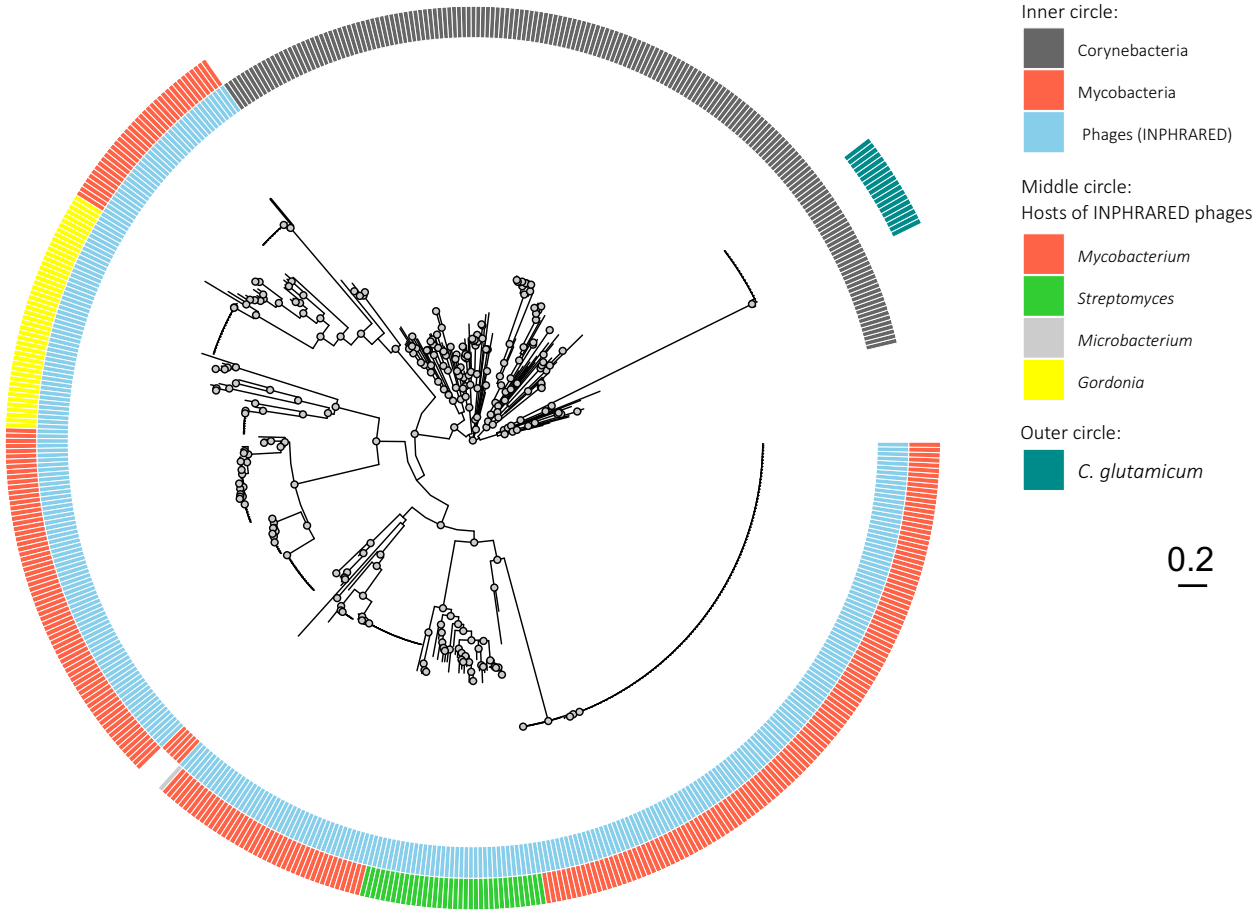

Supplementary Fig. 6 | *C. glutamicum*–encoded Lsr2 forms a distinct clade separate from *Mycobacterium*- and phage-encoded homologs. Midpoint-rooted protein phylogeny of 540 Lsr2 homolog sequences (Supplementary Table 8). The dataset comprises 174 *Corynebacterium* sequences (including 18 *C. glutamicum*), five mycobacterial sequences, and 361 phage-encoded Lsr2 homologs. *C. glutamicum* Lsr2 sequences cluster within the bacterial clade and are clearly separated from phage-encoded Lsr2 homologs. Phage sequences were retrieved from the INPHARED database[1] and include representatives infecting *Mycobacterium*, *Streptomyces*, *Gordonia,* and *Microbacterium*. Bootstrap support values (>70) are indicated by grey circles.

Supplementary Table 1 | Strains used and generated in this study.

Organism	Strains	Characteristics	Reference	Comment
E. coli	DH5α	F- Φ80*lacZ*Δ*M15* Δ(*lacZYA-argF*) *U169 recA1 endA1 hsdR17* (r_K^-, m_K^+) *phoA supE44* thi-1 *gyrA96 relA1* λ^-	Invitrogen (Thermo Fisher Scientific, DE)	
E. coli	BL21(DE3)	F- *ompT* $hsdS_B$(r_B^- m_B^-) *gal dcm* BL21(DE3), protein production host	[2]	
C. glutamicum	ATCC 13032	Wild type, biotin-auxotrophic strain	[3]	In this work named as WT
C. glutamicum	MB001 - (ΔCGP1, 2, 3)	Biotin-auxotrophic strain with deleted prophage clusters CGP1 (cg1507-cg1524), CGP2 (cg1746-cg1752), and CGP3 (cg1890- cg2071)	[4]	In this work named as -CGP3
C. glutamicum	ATCC 13032 ΔcglMRR	ATCC 13032 with in-frame deletion of restriction-modification system cg*MMR* (cg1996-cg1998), located within prophage CGP3	[4]	In this work named as +CGP3
C. glutamicum	+CGP3 *cgpS*-Cstrep	Derivative of +CGP3 Strain with genomic exchange of the *cgpS* gene to *cgpS*-strep, encoding a C-terminal Strep-tag fusion.	This study	
C. glutamicum	D1	Derivative of ATCC 13032 Δcg*MMR* (+CGP3) with deleted CGP3 Region D1 (cg1890 - cg 1895)	This study	
C. glutamicum	D2	Derivative of ATCC 13032 Δcg*MMR* (+CGP3) with deleted CGP3 Region D2 (cg1896 - cg1908)	This study	
C. glutamicum	D3	Derivative of ATCC 13032 Δcg*MMR* (+CGP3) with deleted CGP3 Region D3 (cg1914 - cg1923)	This study	
C. glutamicum	D4	Derivative of ATCC 13032 Δcg*MMR* (+CGP3) with deleted CGP3 Region D4 (cg1924 - cg1937)	This study	
C. glutamicum	D5	Derivative of ATCC 13032 Δcg*MMR* (+CGP3) with deleted CGP3 Region D5 (cg1938 - cg1946)	This study	
C. glutamicum	D6	Derivative of ATCC 13032 Δcg*MMR* (+CGP3) with deleted CGP3 Region D6 (cg1947 - cg1956)	This study	
C. glutamicum	D7	Derivative of ATCC 13032 Δcg*MMR* (+CGP3) with deleted CGP3 Region D7 (cg1957 - cg1962)	This study	
C. glutamicum	D8.1	Derivative of ATCC 13032 Δcg*MMR* (+CGP3) with deleted CGP3 Region D8.1 (cg1963-cg1965)	This study	
C. glutamicum	D8.2	Derivative of ATCC 13032 Δcg*MMR* (+CGP3) with deleted CGP3 Region D8.2 (cg1967-cg1975)	This study	
C. glutamicum	D9	Derivative of ATCC 13032 Δcg*MMR* (+CGP3) with deleted CGP3 Region D9 (cg1976 - cg1983)	This study	
C. glutamicum	D10	Derivative of ATCC 13032 Δcg*MMR* (+CGP3) with deleted CGP3 Region D10 (cg1984 - cg1991)	This study	
C. glutamicum	D11	Derivative of ATCC 13032 Δcg*MMR* (+CGP3) with deleted CGP3 Region D11 (cg1992 - cg1999)	This study	
C. glutamicum	D12	Derivative of ATCC 13032 Δcg*MMR* (+CGP3) with deleted CGP3 Region D12 (cg2000-cg2005)	This study	
C. glutamicum	D13	Derivative of ATCC 13032 Δcg*MMR* (+CGP3) with deleted CGP3 Region D13 (cg2006-cg2011)	This study	
C. glutamicum	D14	Derivative of ATCC 13032 Δcg*MMR* (+CGP3) with deleted CGP3 Region D14 (cg2012-cg2022)	This study	
C. glutamicum	D15	Derivative of ATCC 13032 Δcg*MMR* (+CGP3) with deleted CGP3 Region D15 (cg2023 - cg 2032)	This study	
C. glutamicum	D16	Derivative of ATCC 13032 Δcg*MMR* (+CGP3) with deleted CGP3 Region D16 (cg2032 - cg2037)	This study	
C. glutamicum	D17	Derivative of ATCC 13032 Δcg*MMR* (+CGP3) with deleted CGP3 Region D17 (cg2037 - cg2045)	This study	
C. glutamicum	D18	Derivative of ATCC 13032 Δcg*MMR* (+CGP3) with deleted CGP3 Region D18 (cg2046 - cg2059)	This study	
C. glutamicum	D19	Derivative of ATCC 13032 Δcg*MMR* (+CGP3) with deleted CGP3 Region D19 (cg2059 - cg2064)	This study	
C. glutamicum	D20	Derivative of ATCC 13032 Δcg*MMR* (+CGP3) with deleted CGP3 Region D20 (cg2065 - cg2071)	This study	
C. glutamicum	D30%	Derivative of ATCC 13032 Δcg*MMR* (+CGP3) with deleted CGP3 Region D30% (cg1890 - cg1965)	This study	
C. glutamicum	D70%	Derivative of ATCC 13032 Δcg*MMR* (+CGP3) with deleted CGP3 Region D70% (cg1967 - cg2071)	This study	
CL31		Siphovirus morphology. 45,061 bp. GC content of 54.4%. Genbank: MW582634.1	[5]	
PSOnyx		Siphovirus morphology. 80,277 bp circularly permuted genome. GC content of 53.0%. Genbank: OR521085.1	[6]	
JeanGrey		Myovirus morphology. 106,539 bp circularly permuted genome. GC content of 46.8%. Genbank: PZ176366	This study	

Supplementary Table 2 | Plasmids used and generated in this study.

Plasmid	Characteristics	Reference
pk18/19*mobsacB*	Used for marker-free genomic Integration or Deletion. This plasmid contains a genetically modified *sacB* gene that lacks the *Hind*III and *Eco*RI restriction sites in the coding region for negative selection, a *Kan*^{R} selection marker, and the Rp4 mobilization region. (*oriV*$_{E.c.}$ *lacZα*).	7
pJC1	*Kan*^{R}, *Amp*^{R}; *oriV*$_{C.g.}$, *oriV*$_{E.c.}$; *C. glutamicum*/*E. coli* shuttle vector	8
pAN6	*Kan*R; *C. glutamicum*/*E. coli* shuttle vector for gene expression under control of the tac promoter; (Ptac, lacIq, pBL1 oriVC.g., pUC18 oriVE.c.)	9
pAN6-cgps_Cstrep	Derivative of pAN6 containing the *cgpS* gene without stop codon encoding a C-terminal Strep-tag fusion	10
pk19*mobsacB*:CGP3-D1	Derivative of pk18/19*mobsacB* for Deletion of CGP3 Region D1 (cg1890 - cg 1895)	This Study
pk19*mobsacB*:CGP3-D2	Derivative of pk18/19*mobsacB* for Deletion of CGP3 Region D2 (cg1896 - cg1908)	This Study
pk19*mobsacB*:CGP3-D3	Derivative of pk18/19*mobsacB* for Deletion of CGP3 Region D3 (cg1914 - cg1923)	This Study
pK19_D4	Derivative of pk18/19*mobsacB* for Deletion of CGP3 Region D4 (cg1924 - cg1937)	This Study
pk19*mobsacB*:CGP3-D5	Derivative of pk18/19*mobsacB* for Deletion of CGP3 Region D5 (cg1938 - cg1946)	This Study
pk19*mobsacB*:CGP3-D6	Derivative of pk18/19*mobsacB* for Deletion of CGP3 Region D6 (cg1947 - cg1956)	This Study
pk19*mobsacB*:CGP3-D7	Derivative of pk18/19*mobsacB* for Deletion of CGP3 Region D7 (cg1957 - cg1962)	This Study
pk19*mobsacB*:CGP3-D8.1	Derivative of pk18/19*mobsacB* for Deletion of CGP3 Region D8.1 (cg1963-cg1965)	This Study
pk19*mobsacB*:CGP3-D8.2	Derivative of pk18/19*mobsacB* for Deletion of CGP3 Region D8.2 (cg1967-cg1975)	This Study
pk19*mobsacB*:CGP3-D9	Derivative of pk18/19*mobsacB* for Deletion of CGP3 Region D9 (cg1976 - cg1983)	This Study
pk19*mobsacB*:CGP3-D10	Derivative of pk18/19*mobsacB* for Deletion of CGP3 Region D10 (cg1984 - cg1991)	This Study
pk19*mobsacB*:CGP3-D11	Derivative of pk18/19*mobsacB* for Deletion of CGP3 Region D11 (cg1992 - cg1999)	This Study
pk19*mobsacB*:CGP3-D12	Derivative of pk18/19*mobsacB* for Deletion of CGP3 Region D12 (cg2000-cg2005)	This Study
pk19*mobsacB*:CGP3-D13	Derivative of pk18/19*mobsacB* for Deletion of CGP3 Region D13 (cg2006-cg2011)	This Study
pk19*mobsacB*:CGP3-D14	Derivative of pk18/19*mobsacB* for Deletion of CGP3 Region D14 (cg2012-cg2022)	This Study
pk19*mobsacB*:CGP3-D15	Derivative of pk18/19*mobsacB* for Deletion of CGP3 Region D15 (cg2023 - cg 2032)	This Study
pk19*mobsacB*:CGP3-D16	Derivative of pk18/19*mobsacB* for Deletion of CGP3 Region D16 (cg2032 - cg2037)	This Study
pk19*mobsacB*:CGP3-D17	Derivative of pk18/19*mobsacB* for Deletion of CGP3 Region D17 (cg2037 - cg2045)	This Study
pk19*mobsacB*:CGP3-D18	Derivative of pk18/19*mobsacB* for Deletion of CGP3 Region D18 (cg2046 - cg2059)	This Study
pk19*mobsacB*:CGP3-D19	Derivative of pk18/19*mobsacB* for Deletion of CGP3 Region D19 (cg2059 - cg2064)	This Study
pk19*mobsacB*:CGP3-D20	Derivative of pk18/19*mobsacB* for Deletion of CGP3 Region D20 (cg2065 - cg2071)	This Study
pK19_D1-8.1	Derivative of pk18/19*mobsacB* for Deletion of CGP3 Region D30% (cg1890 - cg1965)	This Study
pK19_D8.2-20	Derivative of pk18/19*mobsacB* for Deletion of CGP3 Region D70% (cg1967 - cg2071)	This Study
pJC1-P$_{jg121}$-*mvenus*	pJC1-P$_{lys}$-*venus* derivative replacing P$_{lys}$ with the region D fused to *mvenus* (BamHI, NdeI); the insert includes the promoter region, 30 bp of the coding sequence, a stop codon, and an additional ribosome binding site (AGGAG) in front of *mvenus*. The vector also includes a terminator sequence from Bacillus subtilis and a *Kan*^{R} marker.	This Study
pJC1-P$_{jg64}$-*mvenus*	pJC1-P$_{lys}$-*venus* derivative replacing P$_{lys}$ with the region B fused to *mvenus* (BamHI, NdeI); the insert includes the promoter region, 30 bp of the coding sequence, a stop codon, and an additional ribosome binding site (AGGAG) in front of *mvenus*. The vector also includes a terminator sequence from Bacillus subtilis and a *Kan*^{R} marker.	This Study
pk19-cg1966:*cgpS*-Cstrep	Derivative of pk18/19*mobsacB* for Integration of Strep tag at the C terminus of *cgpS*, deleting the Stop codon of the gene	This Study
pJC1-P$_{cgpS}$:*cgpS*-Flex-*venus*	pJC1 derivative containing the *cgpS* gene and the promoter P*cgpS* missing the stop codon. A flexible Linker together with the *mvenus* gene.	This Study
pJC1-P$_{divS}$-e2-*crimson*	pJC1 derivative containing the promoter of divS (411 bp) fused to e2-*crimson*; the insert includes the promoter of divS, 30 bp of the coding sequence, a stop codon, and an additional ribosome binding site (pET16) in front of e2-*crimson*	[11]
pJC1- P$_{gntK}$-*venus*	pJC1 derivative containing the promoter of *gntK* fused to *mvenus*; the insert includes the promoter of *gntK*, 30 bp of the coding sequence, a stop codon, and an additional ribosome binding site (AGGAG) in front of *mvenus*	This Study
pJC1-P$_{lys}$-*venus*	This *C. glutamicum* shuttle vector is a modified version of pJC1, which incorporates the 444 bp promoter region of lys gene (cg1974) linked to the *venus* gene via a linker. It contains a stop codon and an artificial RBS (AGGAG). The vector also includes a terminator sequence from Bacillus subtilis and a *Kan*^{R} marker.	[12]

Supplementary Table 3 | Genome annotation of bacteriophage JeanGrey. (a) Final genome annotation including ORF number, strand orientation, start and stop coordinates, ORF length, and predicted function. Predicted transmembrane domains and transcriptional terminators are indicated. Consecutive genes sharing the same color are assigned to putative operons based on RNA-seq data. (b) Predicted phage terminator analysis performed with PhageScope[13] and further validation via RNA Seq profile analysis. (c) tRNA Sequence prediction analysis[14].

(Provided as separate file: Table_S3-Annotation.xlsx)

Supplementary Table 4 | Oligonucleotides used in this study for cloning, sequencing, (RT)-qPCR, and EMSA studies.

(Provided as separate file: Table_S4-Primers.xlsx)

Supplementary Table 5 | Raw values and differential protein abundance during phage infection in-CGP3 (a,c) and +CGP3 (b, d) cells. (a, b)Raw protein abundance values for all samples following filtering based on minimum peptide count criteria. Only proteins supported by at least 2 peptides were retained and classified (0_1-3 for t 0 min; 1_1-4 for t = 15 min 2_1-3 for t 30 min; 3_1-3 for t 60 min). (c, d) Log_2 fold changes represent mean differences between infected and non-infected samples calculated from three independent biological replicates (0_1-3 for t = 0 min; 1_1-4 for t = 15 min 2_1-3 for t = 30 min; 3_1-3 for t = 60 min). Statistical significance (Columns: Student's T-test Significant_0/1/2/3) was determined using two-sided Student's t-tests. Adjusted P values < 0.05 were considered significant.

(Provided as separate file: Table_S5-Proteomics.xlsx)

Supplementary Table 6 | Overview of EMSA analysis of phage DNA regions tested with increasing CgpS concentrations. (a) Characteristics of tested DNA fragments, including average GC content, genomic coordinates, fragment length, primer sequences (see Supplementary Table 4), GC content of the local drop region, and predicted protein–DNA interactions based on AlphaFold modelling using three CgpS monomers and one DNA fragment.

N°	Region	GC Average Fragment	Start	End	Length Fragment	PriF	PriR	GC Drop Region	Interaction via AlphaFold?
1	Region A	40%	1956	2207	252	B171_JG1_for	B172_JG1_rev	25%	possible
2	Region S1	40%	12254	12456	203	B173_JG23_for	B174_JG23_rev	26%	unknown
3	Region B	41%	52003	52215	213	B181_JG83_for	B182_JG83_rev	25%	unknown
4	Region S2	0.42	86603	86840	238	B181_JG83_for	B182_JG83_rev	27%	possible
5	Region D	35%	91055	91248	194	B189_JG121_for	B190_JG121_rev	25%	unknown
6	*cgpS*	32%	1848000	1848388	388	B191_EMSA_*cgps*_for	B192_EMSA_*cgps*_rev	28%	Yes - control
7	*gntK*	48%	2602000	2602275	253	B193_EMSA_*gntK*_for	B194_EMSA_*gntK*_rev	43%	No – control

Supplementary Table 7 | RNA-seq analysis across all targets and time points. (a) Sample overview including strain background and infection conditions. (b–c) Log_2 fold changes for-CGP3 cells under infection. (d–f) Log_2 fold changes for +CGP3 cells under infection. Differential expression values were filtered using the following criteria: maximum group mean > 10, false discovery rate (FDR) < 0.05, and log_2 fold change > 1 (overexpression) and log_2 fold change < 1 (reductions). (g–i) Transcript abundance values (TPM) for all genes across all time points without filtering. For each sample, total transcript counts, RPKM, TPM, and CPM values are provided.

(Provided as separate file: Table_S7-RNASeq_Statistics.xlsx)

Supplementary Table 8 | Genome sequences encoding Lsr2 homologues included in phylogenetic analysis. For each candidate, the table lists the genome ID, locus tag and protein accession of the Lsr2 homologue, source organism, genome or contig length, and strain designation. These sequences were used to construct the phylogenetic tree shown in Supplementary Figure 6.

(Provided as separate file: Table_S8_ls2_genomes.xlsx)

Supplementary Table 9 | Annotation of genomic regions encoding Lsr2 homologues. For each candidate, the table lists the genome ID, Lsr2 locus identifier, genomic start and end coordinates, protein accession number, and protein length (amino acids). Surrounding regions were analyzed for the presence of conjugative elements (ConjScan), defense-related proteins (DefenseFinder), and complete defense systems (annotated defense type). These data was used to complete Figure 4,b and Figure 4,c.

(Provided as separate file: Table_S9_lsr2_regions.xlsx)

Supplementary Video 1. Time-lapse imaging of-CGP3 infection with JeanGrey. Three-hour time-lapse of-CGP3 cells on 1.5% LB agar following infection with JeanGrey. An overnight culture was diluted to an OD_{600} of 0.2 and pre-incubated with phage at a multiplicity of infection (MOI) of 1 for 20 min prior to imaging. Images were acquired every 3 min. Scale bar of 10 μm.

(Provided as separate file: SuppVideo1_minusCGP3_3h.avi)

Supplementary Video 2. Time-lapse imaging of +CGP3 infection with JeanGrey. Three-hour time-lapse of +CGP3 cells on 1.5% LB agar following infection with JeanGrey. An overnight culture was diluted to an OD_{600} of 0.2 and pre-incubated with phage at a multiplicity of infection (MOI) of 1 for 20 min prior to imaging. Images were acquired every 3 min. Scale bar of 10 μm.

(Provided as separate file: SuppVideo2_plusCGP3_3h.avi)

References:

1 Cook, R. *et al.* INfrastructure for a PHAge REference Database: Identification of Large-Scale Biases in the Current Collection of Cultured Phage Genomes. *Phage (New Rochelle)* **2**, 214–223 (2021). https://doi.org/10.1089/phage.2021.0007

2 Studier, F. W. & Moffatt, B. A. Use of bacteriophage T7 RNA polymerase to direct selective high-level expression of cloned genes. *J Mol Biol* **189**, 113–130 (1986). https://doi.org/10.1016/0022-2836(86)90385-2

3 Kinoshita, S., Udaka, S. & Shimono, M. Studies on the amino acid fermentation. Part 1. Production of L-glutamic acid by various microorganisms. *J Gen Appl Microbiol* **50**, 331–343 (2004).

4 Baumgart, M. *et al.* Construction of a prophage-free variant of Corynebacterium glutamicum ATCC 13032 for use as a platform strain for basic research and industrial biotechnology. *Appl Environ Microbiol* **79**, 6006–6015 (2013). https://doi.org/10.1128/AEM.01634-13

5 Hunnefeld, M. *et al.* Genome Sequence of the Bacteriophage CL31 and Interaction with the Host Strain *Corynebacterium glutamicum* ATCC 13032. *Viruses* **13** (2021). https://doi.org/10.3390/v13030495

6 Rossier, O. *et al.* Genome sequence of PSonyx, a singleton bacteriophage infecting Corynebacterium glutamicum. *Microbiol Resour Announc* **13**, e0115523 (2024). https://doi.org/10.1128/mra.01155-23

7 Schafer, A. *et al.* Small mobilizable multi-purpose cloning vectors derived from the Escherichia coli plasmids pK18 and pK19: selection of defined deletions in the chromosome of Corynebacterium glutamicum. *Gene* **145**, 69–73 (1994). https://doi.org/10.1016/0378-1119(94)90324-7

8 Cremer, J., Eggeling, L. & Sahm, H. CLONING THE DAPA DAPB CLUSTER OF THE LYSINE-SECRETING BACTERIUM CORYNEBACTERIUM-GLUTAMICUM. *Molecular and General Genetics* **220**, 478–480 (1990). https://doi.org/10.1007/bf00391757

9 Frunzke, J., Engels, V., Hasenbein, S., Gatgens, C. & Bott, M. Co-ordinated regulation of gluconate catabolism and glucose uptake in Corynebacterium glutamicum by two functionally equivalent transcriptional regulators, GntR1 and GntR2. *Molecular Microbiology* **67**, 305–322 (2008). https://doi.org/10.1111/j.1365-2958.2007.06020.x

10 Pfeifer, E. *et al.* Silencing of cryptic prophages in Corynebacterium glutamicum. *Nucleic Acids Research* **44**, 10117–10131 (2016). https://doi.org/10.1093/nar/gkw692

11 Nanda, A. M. *et al.* Analysis of SOS-induced spontaneous prophage induction in Corynebacterium glutamicum at the single-cell level. *J Bacteriol* **196**, 180–188 (2014). https://doi.org/10.1128/JB.01018-13

12 Wiechert, J. *et al.* CRISPR/dCas-mediated counter-silencing: reprogramming dCas proteins into antagonists of xenogeneic silencers. *mBio* **16**, e0038225 (2025). https://doi.org/10.1128/mbio.00382-25

13 Wang, R. H. *et al.* PhageScope: a well-annotated bacteriophage database with automatic analyses and visualizations. *Nucleic Acids Res* **52**, D756–D761 (2024). https://doi.org/10.1093/nar/gkad979

14 Chan, P. P., Lin, B. Y., Mak, A. J. & Lowe, T. M. tRNAscan-SE 2.0: improved detection and functional classification of transfer RNA genes. *Nucleic Acids Res* **49**, 9077–9096 (2021). https://doi.org/10.1093/nar/gkab688